4 LZ Sensitivity

The LZ detector system described in previous and subsequent chapters is highly sensitive to a variety of physics signals. The principal signal we seek is that of NRs distributed uniformly throughout the LXe TPC volume, in response to an impinging flux of nonrelativistic galactic WIMPs. In the first sections of this chapter, we describe the sensitivity to various WIMP-particle cross sections.

The first step in selecting the sample of WIMP candidates is to define a suitable search region in the two variables: S1 (the prompt scintillation light) and S2 (the delayed electroluminescence light, a measure of primary ionization). The use of both variables enables the separation of NRs from the much more numerous ERs, resulting in a search region that is nearly or completely background-free for a multitonne Xe fiducial mass. The second step is to remove from this sample all events associated with time-coincident energy deposit in the Xe skin or the outer detector.

We first describe our sensitivity and discovery potential for the spin-independent (SI) interpretation of the WIMP-nucleon interaction. We then discuss interpretations involving more general forms of the WIMP-nucleon interaction.

The S2 signal is sensitive to smaller energy depositions than is S1 and, as described in Chapter 3, NR thresholds <1 keV can be sensed in the ionization channel due to its sensitivity to individual electrons emitted from the liquid. Use of the S2 signal alone, when the NR is too feeble to cause a detectable S1, can provide enhanced sensitivity to WIMPs of the lowest mass, which cause the softest NR spectra. Use of the S2 signal alone removes the capability to distinguish NRs from ERs, and consequently the ERs provide a substantial and irreducible background to the "S2-only" analysis. We note, however, that this is true of other WIMP-search technologies (e.g., p-type point-contact germanium detectors) that are also searching for light WIMPs. We estimate the limiting sensitivity of an "S2-only" analysis of LZ data.

Should LZ see a WIMP signal, the distribution of that signal in NR energy will allow constraints on the WIMP-Xe scattering cross section, the WIMP-Xe reduced mass, and on the velocity distribution of galactic WIMPs [1].

A variety of other physics processes can be probed by selective detection of NRs and ERs as defined with S1 and S2. The central fiducial region of the LZ detector will be an extraordinarily quiet laboratory for processes that deposit energy. Among the physics processes that can be probed are:

1. Interactions of WIMPs with atomic electrons.
2. Solar and certain dark-matter axion-like particles (ALPs), which interact via the axioelectric effect.
3. Solar neutrinos emitted by the pp fusion process in the sun.
4. Neutrinos emitted by a nearby supernova and detected by coherent neutrino-nucleus scattering.
5. Neutrinoless double-beta decay of ^{136}Xe.
6. Neutrino oscillations with parameters motivated by the current "reactor/source anomalies," and a neutrino magnetic moment.

We also present a summary of top-level requirements at the end of this chapter. We have a well-developed process to capture and flow down science requirements. The dependencies of key requirements on critical performance characteristics are also summarized.

4.1 WIMP Sensitivity and Discovery Potential

The principal physics analyses of the LZ experiment will be searches for the recoils of Xe atoms caused by the interaction of WIMPs with the Xe nucleus. As discussed above, two types of signal are formed in the LXe response to the recoils: S1 and S2. In the principal LZ search, the energy of the recoil is reconstructed from a combination of S1 and S2, and the ratio S2/S1 provides discrimination of NRs from

the background of ERs. The value of the reconstructed energy depends on whether the event is an NR or an ER.

An auxiliary LZ search for NRs exploits the S2 signal alone (the S2-only analysis), which is more sensitive to energy deposits than is the S1 signal. The S2-only analysis provides additional sensitivity to small energy deposits from low-mass WIMPs, at the cost of the ability to discriminate against the ER background.

4.1.1 S1+S2 Analysis

The S1+S2 analysis in LZ will follow the general framework of the published first LUX search for NRs in response to WIMPs [2]. The experimental details that influence the analysis were discussed in Chapter 3. We define a search region in the plane of log(S2/S1) versus S1, shown in Figure 4.1.1.1. The definition of the LZ baseline search region in this plane is described in Table 4.1.1.1.

The baseline detector performance assumed for LZ is in most cases more conservative than that achieved by LUX. The most prominent exception

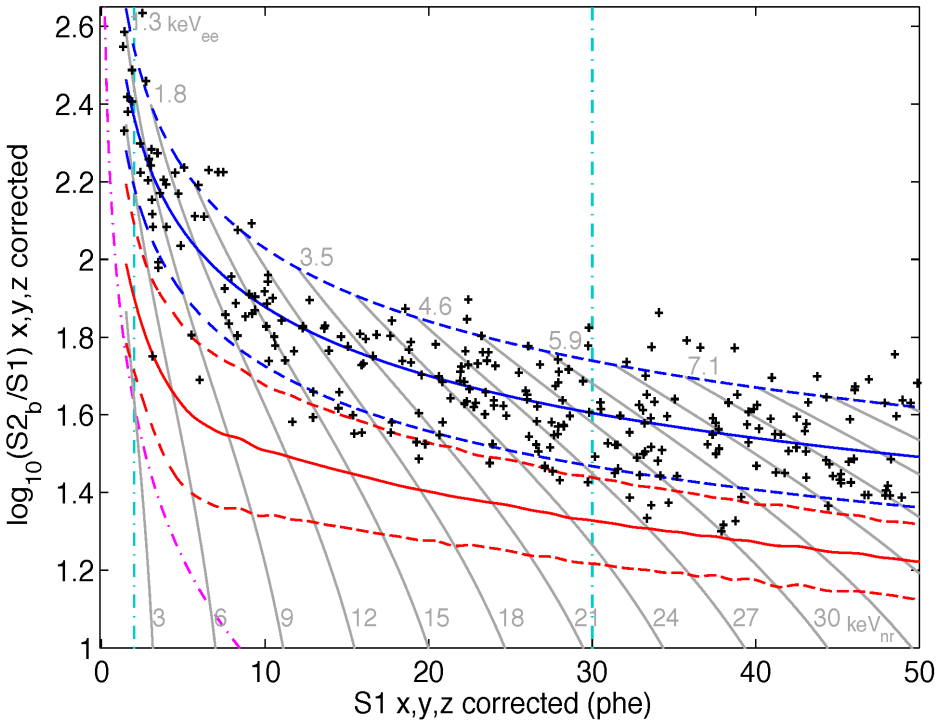

Figure 4.1.1.1. The LUX WIMP search data [2]. The logarithm of the ratio S2/S1 is plotted versus S1, after spatial corrections. The centroid (solid) and search region boundaries (dotted) are red for the signal (NR) region or "band," and corresponding lines in blue describe the primary background (ER) band. The dotted lines are $\pm 1.28\sigma$ around the centroid. Contours of equal recoil energy for NR (keV$_{nr}$) and ER (keV$_{ee}$) interpretations are shown in grey. The LUX data, consistent with a background of ERs, is shown, and the LUX NR search region is between the vertical light-blue dot-dash lines and the solid red and dashed red lines.

Table 4.1.1.1. Comparison of the key performance assumptions for LZ compared to published values for LUX.

Quantity	Units	LZ Assumption	LUX [2]
Recoil threshold, 50% efficiency	keV$_{nr}$	6	4.3
Maximum recoil energy	keV$_{nr}$	30	n/a
S1 range	Detected photoelectrons	3-30	2-30
S2 range	Detected photoelectrons	>250	>200
S1 light-collection efficiency	Absolute	7.5%	14%
Photocathode efficiency	Absolute	25%	30%
Liquid/gas emission probability	Absolute	>95%	65%
ER discrimination	Absolute	99.5%	99.6%
NR acceptance assumed for sensitivity estimation	Absolute	50%	50%

in Table 4.1.1.1 is the liquid/gas emission probability, where we presume that the limitations of the LUX electric field will be removed in the LZ experiment. In practice, the NR acceptance exceeds 50% for the lowest-energy ERs, but we make a conservative assumption that the acceptance is 50%.

The benchmark process we will use to interpret NRs will be the interaction of WIMPs via an SI process, such as exchange of a Higgs particle [3], with the gluons in the nucleons in the Xe nucleus [4]. This process produces a WIMP-nucleus scattering rate that is independent of the identity, neutron or proton, of the nucleon in the nucleus. For the low-momentum transfers of typical WIMP interactions, the scattering amplitude is proportional to A, the number of nucleons in the nucleus. The scattering cross section includes the density of states, which also favors larger A, while the threshold for energy detection favors smaller A. The nuclear form factor is employed to account for quantum-mechanical interference attributable to the non-zero nuclear size [6], and the standard halo model (SHM) of the distribution of WIMP velocities in the Milky Way is used [7].

The backgrounds expected for LZ are described in detail in Chapter 12 and summarized in Table 3.8.1.1. A background arises from solar-neutrino-induced ERs that leak into the NR region. In the ER band and energy range of 1.5-6.5 keV_{ee}, we expect ERs from neutrinos originating predominantly in the pp fusion process in the sun, and scattering in LZ off of atomic electrons. The flux of pp neutrinos is predicted by solar models to better than 1%, assuming the solar

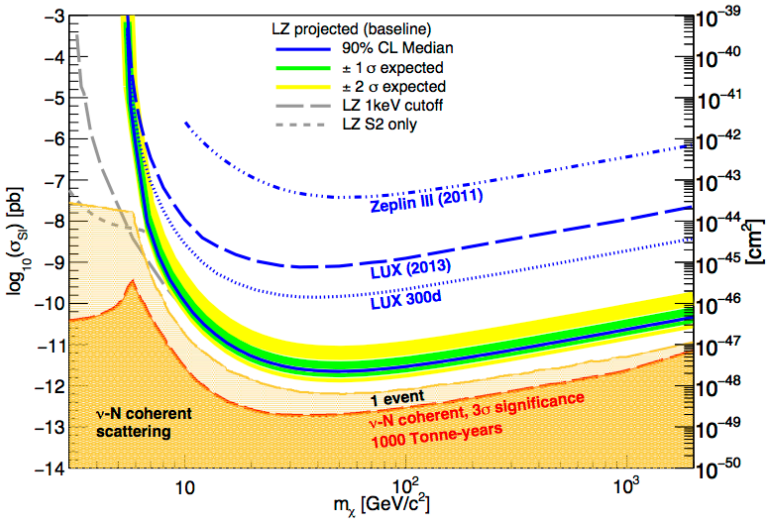

Figure 4.1.1.2. Projected 90% confidence level (CL) sensitivity for the SI WIMP-nucleon cross sections for LZ (solid blue) along with the current world's-best limits from LUX (dashed blue), the LUX 300-day projection (dotted blue), and the final ZEPLIN result (dot-dashed blue). Regions above the curves are excluded. The green and yellow bands display the 68% (1σ) and 95% (2σ) ranges of the expected LZ 90% CL limit. The grey small-dashed line is an estimate of the 90% CL for the S2-only technique. The grey long-dashed line indicates the potential improved low-mass reach if the lower energy threshold is lowered. The regions where background NRs from cosmic neutrinos emerge, and an ultimate neutrino floor [5], are shown.

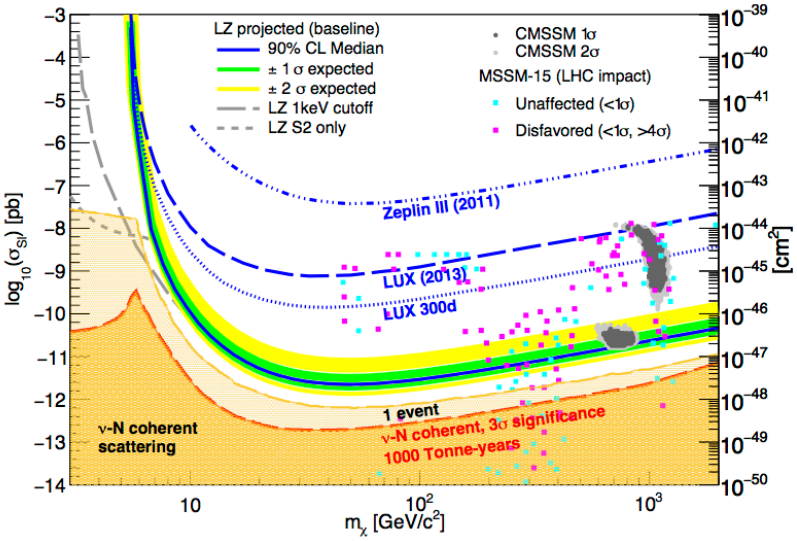

Figure 4.1.1.3. The same, in part, information as Figure 4.1.1.2, very recent SUSY theoretical expectations included. The grey-colored regions are favored by recent scans of the five-parameter CMSSM, which include the most current constraints from LHC results [8]. The purple and blue points are pMSSM models, where 15 parameters are scanned [9]. The number of standard deviations (σ) that quantify consistency are higher for models that are more inconsistent with very recent LHC data.

luminosity constraint, but there is uncertainty that arises from atomic binding effects of electrons in the Xe atom. The ultimate level of ERs from solar neutrinos in the LXe TPC will be well constrained by studies of the "sideband" in ER energy extending from 6.5–20 keV_{ee}. For energies above 20 keV_{ee}, ERs from the 2ν double-beta decay from ^{136}Xe dominate the spectrum of ER events.

Another source of background is the as-yet-unobserved coherent nuclear scattering from atmospheric neutrinos and neutrinos from the diffuse supernova neutrino background (DSNB), which contribute events in the NR band. Nuclear recoils from the coherent scattering of solar neutrinos fall below the LZ energy threshold for the standard S1+S2 analysis.

An additional source of background is beta-decay electrons, generating ERs, emitted from ^{85}Kr and the ^{222}Rn chain. The ultimate level of radon in the TPC will be very well constrained by the measurement of alpha-particles in the radon decay chain.

We use the backgrounds described in Chapter 12 and summarized in Table 3.8.1.1 to derive the projected sensitivity of LZ to WIMPs. The resulting sensitivity plot is shown in Figure 4.1.1.2, along with the current LUX limit and the projected LUX sensitivity. The best (lowest) sensitivity shown, at a mass of approximately 50 GeV/c^2, is about 2 ×10^{-48} cm^2, which is 2 ×10^{-12} pb.

Figure 4.1.1.3 redisplays the information in Figure 4.1.1.2, but includes regions and points in the same parameter space that are consistent with very recent evaluations made with SUSY models, which have included the most recent constraints on those models by LHC experiments. A tightly constrained SUSY model with only five parameters, known as the constrained minimal supersymmetric model (CMSSM), favors WIMP masses and WIMP-nucleon scattering cross sections that are largely within the sensitivity of LZ [8]. These CMSSM models are generally out of reach of future LHC runs, but future gamma-ray telescopes could make a detection complementary to one made by LZ. Figure 4.1.1.3 also shows points that arise from an analysis of a much-less-restricted ensemble of SUSY models, the 15-parameter pMSSM [9] (there is also a 19-parameter phenomenological MSSM [pMSSM] discussed in Chapter 1). For the 15-parameter pMSSM, the recent LHC results have been largely inconsistent with many models that predict WIMP-nucleon cross sections well below the LZ sensitivity.

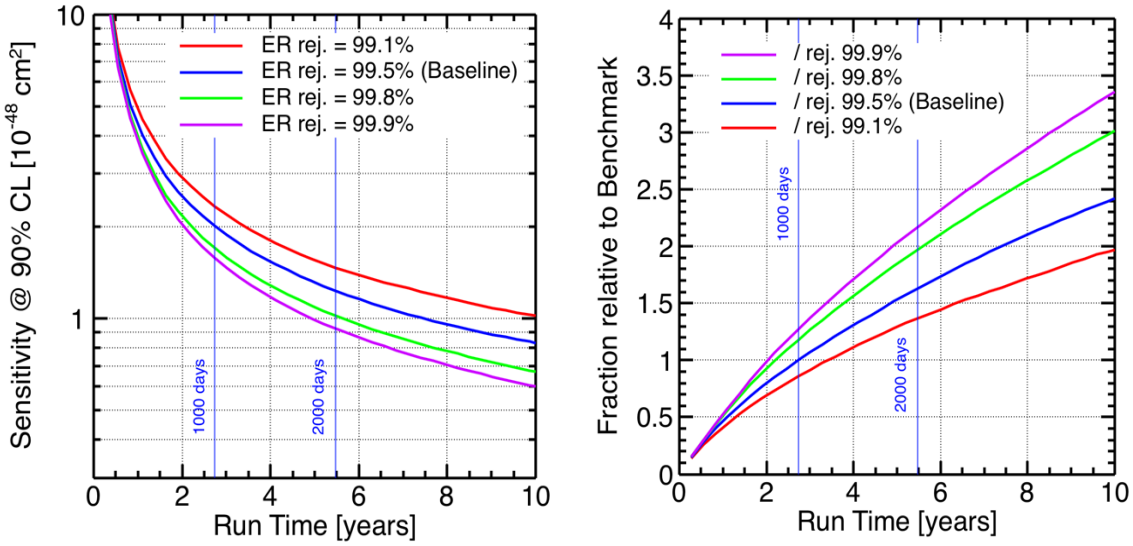

Figure 4.1.1.4. Sensitivity as a function of running time. The left panel shows the 90% CL upper limit on the SI WIMP-nucleon cross section that can be achieved by LZ as a function of exposure in years. The baseline case is blue. The limiting background is misidentification of ERs, which originate principally from solar neutrinos. Improvement of the ER rejection permits improvement between 1,000 and 2,000 live days that is close to the inverse of the time. The right panel shows the improvement relative to the baseline case, which is normalized to 1 unit at 1,000 days exposure.

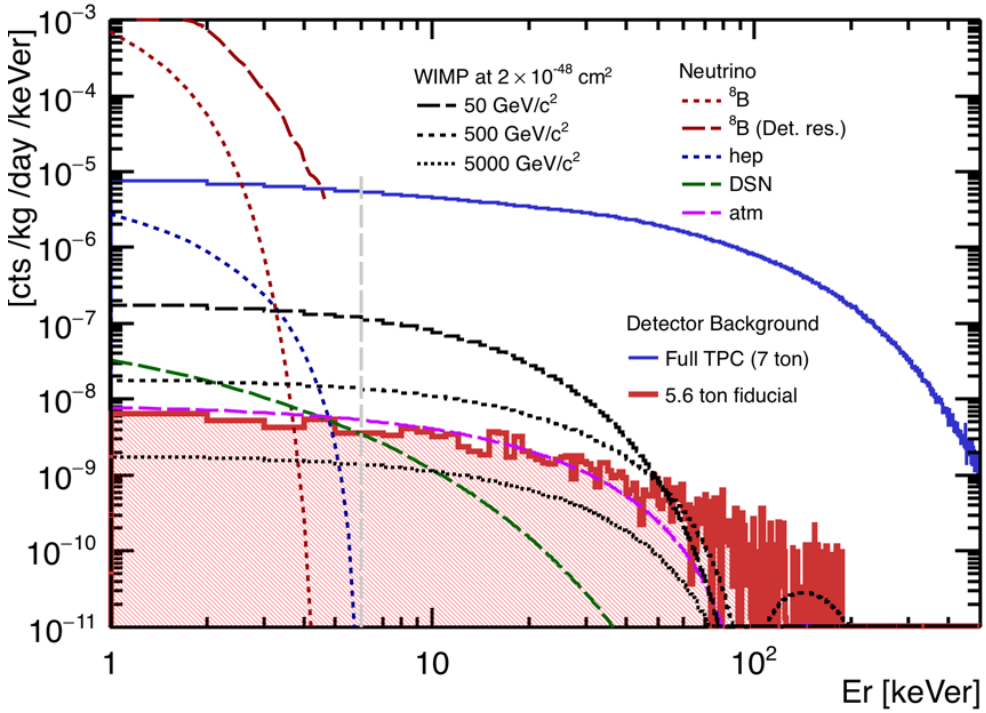

Figure 4.1.1.5. Energy spectra of signal and backgrounds, in the NR band. The expected counts per keV$_{nr}$ per tonne per 1,000 days is shown versus the NR energy. The expected signals from WIMPs of three masses and cross sections are plotted in black. The signal expected from the coherent scattering of solar ^{8}B neutrinos is shown in dotted brown; the dashed brown is after convolution with the expected energy resolution. The LZ threshold is shown in grey dash. Expected signals from coherent nuclear scattering of the diffuse supernova neutrino background (green) and from atmospheric neutrinos (magenta) are shown. The background from external radioactivity in the complete LXe volume is shown in blue, and the portion that survives to the 5.6-tonne fiducial volume is shown in red. The ER rejection is assumed to be the LZ baseline of 99.5%. Contributions from leakage of ERs from pp neutrinos, double-beta decay, ^{222}Rn, and ^{85}Kr are not shown.

The sensitivity of LZ to SI WIMP-nucleon scattering as a function of running time of the experiment is shown in Figure 4.1.1.4, for the three different cases of ER leakage probability into the NR signal region presented in Table 4.1.1.2, and for the ER leakage probability achieved by the ZEPLIN-III experiment. The main physical difference between the LZ baseline, shown in blue, and the case of the ZEPLIN-III ER leakage probability are mainly events from ER leakage.

With twice the live time, the sensitivity at 50 GeV/c^2 improves by about 40%. The scaling of the sensitivity with exposure is less than linear, ultimately limited by backgrounds. If better ER discrimination than 99.5% can be achieved, backgrounds would be reduced and the sensitivity improved. With the longer exposure and the highest discrimination, the 90% CL sensitivity could become about 1 × 10^{-48} cm^2. The energy spectra from potential signals and many of the expected backgrounds are shown in Figure 4.1.1.5 for baseline assumptions.

4.1.2 S2-only Analysis

The center of the LZ LXe volume is very well shielded from gamma rays and neutrons that originate from radioactive impurities outside. The rate of events in the center, measured with either S1 or S2, provides an interesting measurement of impinging particles that do not originate locally. The energy threshold for a detected S2 signal is somewhat lower than that for S1, because electroluminescence provides an amplification mechanism such that a signal electron is well above threshold. For this reason, an analysis using only S2 signals can probe lower energy deposits than one using both S1 and S2.

Because there is no discrimination between NR and ER events when the S2 signal alone is used, the background level in an S2-only search is higher than in the standard S1+S2 analysis. Nevertheless, at the smallest WIMP masses, the S2-only search can provide better sensitivity than the S1+S2 analysis, as depicted in Figure 4.1.1.2.

The S2-only analysis for Figure 4.1.1.2 uses a smaller fiducial mass of 1 tonne, and a threshold of 2.5 ionization electrons extracted from the LXe, which corresponds to 100 phe detected in the Xe PMT system. The reduction of fiducial mass is achieved by requiring the S2 pulse to fall within a radius of 40 cm.

The z-coordinate of the S2 pulse cannot be reconstructed from drift time because of the absence of the S1 pulse from which the start time is determined. However, the electrons in the S2 pulse diffuse as they drift to the cathode, and so the width of the pulse can be used to deduce the z-coordinate of the event, with a resolution of about 10 cm. The reconstruction of the z-coordinate is most effective for events with the shortest drift distance, at the top of the LXe TPC. We assume that the 40 cm closest to the top of the TPC and the 40 cm at the bottom of the TPC will be rejected, resulting in a column height of 70 cm for the fiducial volume.

The principal limitations of the S2-only analysis are instrumental backgrounds that are difficult to extrapolate from the ZEPLIN program and from LUX to LZ. Bursts of ionization electrons take place in LXe TPCs [10]. The origin of these bursts is not yet fully understood, but is likely to be related to electrons trapped on the liquid-vapor interface, vacuum ultraviolet (VUV) light emitted from electroluminescence in the vapor, phosphorescence in materials local to the TPC, and field emission from the cathode. As part of the LZ program, we plan to characterize the contributions of these phenomena. The experience in LUX has been that these bursts can be identified and removed with a loss of live time of approximately 15%.

For the estimate of the S2-only sensitivity in Figure 4.1.1.2, we have neglected instrumental backgrounds. Our experience in LUX indicates that at a threshold of 2.5 ionization electrons, these backgrounds should not be dominant.

4.1.3 General WIMP-Nucleon Couplings

Although the SI coupling provides an important standard for interpreting experimental results, it is one of many possible WIMP-nucleon couplings. Two long-standing themes have guided alternate interpretations: first, that the WIMP-neutron and WIMP-proton couplings, SI or otherwise, might differ; second, that the couplings might involve the spins of the nucleons. For two decades, experimental interpretations of NR experiments have employed the limit where the nucleons are taken to be static, and the WIMP is nonrelativistic. In this “static-nucleon” limit, two classes of terms survive: (1) SI terms, with contributions from scalar, vector, and tensor interactions; and (2) spin-dependent (SD) terms, with a contribution from the axial vector interaction [11].

Recently, the fact that the nucleon velocity is near-relativistic has been applied to the WIMP-nucleus interaction and has led to consideration of couplings that involve the orbital angular momentum of the nucleon [12].

No single target material possesses sensitivity to the complete set of generalized WIMP-nucleon couplings. Xe is sensitive to a wide variety of the general couplings, and targets such as fluorine, sodium, and iodine complement Xe by providing sensitivity to interactions that couple exclusively to proton spin and angular momentum. Should a WIMP signal be seen in LZ, it would be possible to exchange the target of natural Xe with one of isotopically enriched or depleted Xe, to deduce whether the WIMP-nucleon coupling is SI, SD, or something more complex.

Within the context of SI interactions, the coupling coefficient (f_p) to protons may be different from that (f_n) to neutrons. For example, if WIMPs interact via the vector current that results from exchange of the

Z^0, $f_p/f_n = -(1-4\sin^2\theta_w) \simeq -0.04$, and the coupling is SI [13]; this possibility tends to be neglected, because the most-favored models specify that the WIMP is a Majorana fermion, for which the vector current vanishes. A variety of extensions to the Standard Model, including most implementations of SUSY, do result in $f_p \simeq f_n$ for scalar interactions of Majorana fermions, but there are alternates that violate that near-equality [14,15].

The experimental consequences of $f_p \neq f_n$ have recently been examined in depth [16]. Natural Xe has an advantage due to its variety of stable isotopes: Each of seven isotopes constitutes more than 1% of natural Xe. If a signal is seen with any other target, the variety of isotopes in natural Xe makes it impossible to completely suppress its SI interaction cross section by adjusting f_p/f_n to achieve destructive interference. Complete suppression is only possible for elements that consist of a single isotope.

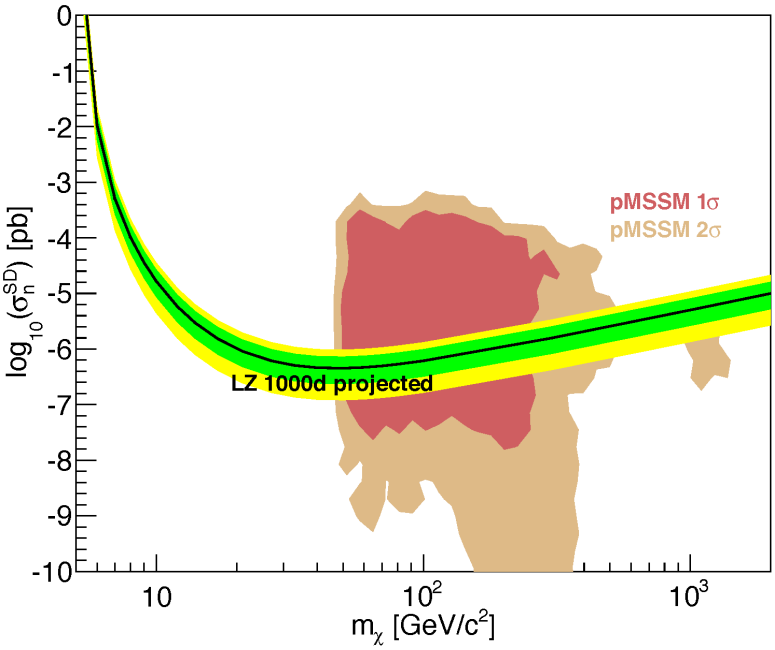

Figure 4.1.3.1. The LZ projected sensitivity to an SD WIMP-neutron interaction. The median LZ 90% CL sensitivity is in black, and the green and yellow bands display the range of 68% (1σ) and 95% (2σ) of the expected 90% CL limits. A fiducial mass of 5.6 tonnes and a live time of 1,000 days is assumed. Expectations from the 15-parameter pMSSM are shown in rose and beige, prior to consideration of the latest LHC constraints [9]. 1 picobarn is 10^{-36} cm^2.

Targets such as argon, iodine, fluorine, and neon do consist dominantly of a signal isotope. It is possible to completely suppress, through a devious choice of f_p/f_n, WIMP interaction rates in these targets, should a signal be seen in another target. Conversely, should a signal be seen in argon, iodine, fluorine, or neon, a sensitivity in Xe that exceeds the isospin-conserving SI interpretation by factors of 40, 2, 90, or 170 would conclusively test the isospin-violating SI interpretation. The large fiducial mass of LZ enables the achievement of these sensitivities relative to experiments with other targets [17].

An SD interaction arises if the WIMP is a Majorana fermion, as expected in most implementations of SUSY, and if the dominant WIMP-quark interaction proceeds through the Z^0. The coupling coefficient (a_p) to proton spin and that (a_n) to neutron spin would be in proportion $a_p/a_n \simeq -1.14$ [15]. Implementations of SUSY can result in a very wide range of values for a_p/a_n [18]. Because most of the neutrons and protons in a nucleus form spin-coupled pairs, the dominant interaction, when possible, arises with an unpaired (odd) neutron or proton. The SD interaction thus fails to benefit from the quantum coherence over nucleons, which greatly enhances the WIMP-nucleus SI cross-section. Nevertheless, the SI and SD WIMP-nucleus cross sections can be, in some cases, of similar magnitude [14].

In the static-nucleon limit, the sensitivity of a Xe target to SD interactions arises primarily from the two isotopes ^{129}Xe and ^{131}Xe, which have unpaired neutrons. These isotopes make up nearly half of natural abundance. There is also sensitivity to SD coupling to the spin of the proton, but this sensitivity is suppressed because the protons in Xe are all paired.

For a given experimental run using natural Xe, the limit for the SD WIMP-neutron cross section is about 10^5 times weaker than the corresponding limit for the isospin-conserving SI cross section. The coherence in the SI case provides the additional sensitivity. To evaluate the LZ sensitivity, we employee the SD

form factors of Ref. [19]. There is an uncertainty due to form-factor variation of a factor of 2 documented in the literature [20], but Ref. [19] uses a recent large-scale nuclear structure calculation to achieve an error at the 10% level. A 1,000-day LZ run would provide a maximum sensitivity to the WIMP-neutron SD cross section of 4×10^{-43} cm^2 for a WIMP mass near 50 GeV/c^2. We portray the expected LZ mass-dependent WIMP-neutron cross-section sensitivity in Figure 4.1.3.2. Additional important sensitivity to a WIMP-neutron SD cross section arises from inelastic scattering with the ^{129}Xe and ^{131}Xe isotopes [21].

When the WIMP-neutron and WIMP-proton cross sections are nearly equal [15], the LZ sensitivity to SD interactions will exceed the current sensitivity of the IceCube and Super-Kamiokande detectors to the annihilation of WIMPs in our sun by 2 orders of magnitude [22,23].

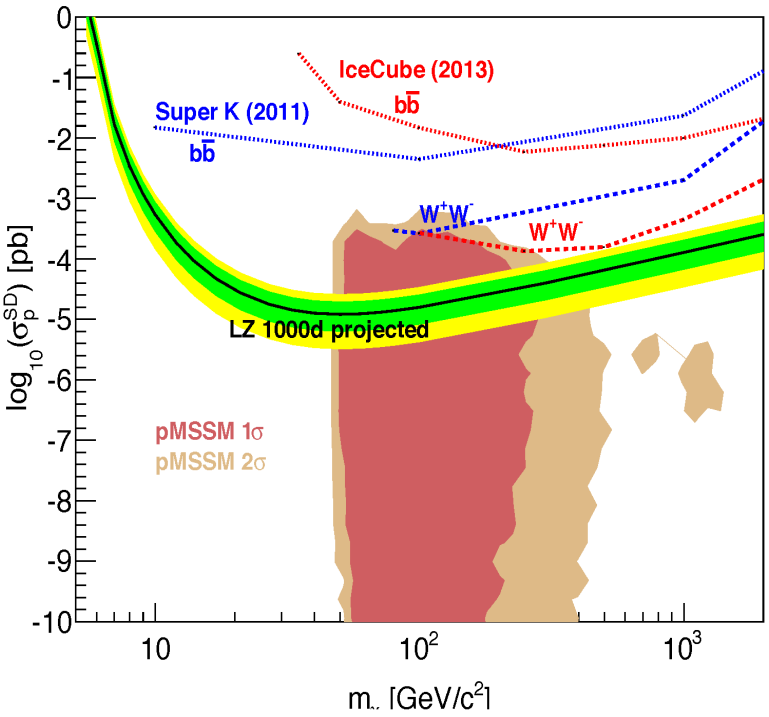

Figure 4.1.3.2. The LZ projected sensitivity to an SD WIMP-proton interaction. The median LZ 90% CL sensitivity is in black, and the green and yellow bands display the range of 68% (1σ) and 95% (2σ) of the expected 90% CL limits. A fiducial mass of 5.6 tonnes and a running time of 1,000 days is assumed. Current indirect detection results from Super-Kamiokande [22] and IceCube [23] are shown. Expectations from the 15-parameter pMSSM are shown in rose and beige, prior to consideration of the latest LHC constraints [9]. 1 picobarn is 10^{-36} cm^2.

If WIMP-Xe scattering is driven by the SD WIMP-proton interaction, and because there are no unpaired proton spins in Xe, the net scattering amplitude can nearly vanish. To evaluate the LZ sensitivity, we employee the SD form factors of Ref. [19], and note that an uncertainty of a factor of 10^3 is documented in the literature [20]. However, Ref. [19] uses a large-scale nuclear structure calculation to achieve an error at the 50% level. The greatest sensitivity of a 1,000-day LZ run, at a WIMP mass near 50 GeV/c^2, would be about 1×10^{-41} cm^2, somewhat better than the current sensitivity of the IceCube or Super-Kamiokande detectors to the annihilation of WIMPs in our sun [22,23].

Recently, the validity of the static-nucleon limit has been examined and found to be substantially incomplete [12]. Ref. [12] employs effective field theory to analyze all the Lorentz structures that can contribute to WIMP-nucleus scattering. In addition to the long-considered SI interactions, the relativistic motion of the nucleons induces three additional terms:

1. An orbital angular-momentum (L) dependent (LD) term.
2. A combined angular-momentum (L) and spin (S) dependent (LSD) term. This term is particularly interesting because its contribution builds coherently among nucleons, like the SI term.
3. The SD term breaks into two independent terms, one transverse and one longitudinal to the momentum transfer.

The five terms can be distinct for neutrons and for protons, resulting in a total of 10 coefficients to completely specify the WIMP-nucleus interaction. Among the targets considered in [12], Xe provides sensitivities to the broadest range of the 10 WIMP-nucleus parameters. For five of those parameters, Xe

gives the best sensitivity per kilogram, and sensitivity is meager for only three of the parameters. Targets that complement a measurement in Xe include fluorine, sodium, and iodine, all of which have an unpaired proton. Analyses of existing experimental constraints based on effective field theory are now under way [24,25].

4.2 Beyond Nuclear Recoils from WIMPs

4.2.1 Electrophilic WIMPs

One type of WIMP-matter coupling that does not cause NRs, at least at tree-level, is the coupling of a WIMP to a charged lepton. A WIMP-charged lepton vector coupling induces a WIMP-nucleon interaction at one loop in perturbation theory, where the charged lepton loop interacts with the nucleon via photon exchanges [26]. This interaction is surprisingly sensitive. The WIMP-nucleon SI cross-section sensitivity of 2×10^{-48} cm^2 achievable by LZ at a WIMP mass of 50 GeV/c^2 corresponds, when converted via a one-loop calculation, to a WIMP-electron cross section of 1×10^{-50} cm^2. Should the interaction be exclusively WIMP-muon, the LZ sensitivity at 50 GeV/c^2 corresponds to a vector-mediated WIMP-muon cross section of 4×10^{-50} cm^2; for a tau, the corresponding WIMP-tau cross section is 3×10^{-49} cm^2.

If the WIMP is a Majorana particle, all its vector couplings vanish, but an SD axial-vector coupling is still possible. The axial-vector coupling does not induce an interaction at higher order in perturbation theory with the nucleus; the only observable consequence in LZ of an axial-vector coupling of a WIMP to an electron is WIMP-electron scattering.

The physical situation for WIMP-electron scattering resembles that for WIMP-nucleon scattering, described at the end of Section 4.1.5, where the nucleon motion is important. The electron motion in the atom is crucial, and it is the very highest momentum tails of the electron wavefunction that determine the cross section for an impinging WIMP to ionize a Xe atom. The resulting events are ERs, and their energy spectrum rises very quickly as the energy deposition falls. Limits on axial-vector WIMP-electron scattering depend critically on the low energy threshold [26].

Interpretations of the DAMA [27] event excess as axial-vector WIMP-electron scattering imply a WIMP-electron cross section of 2×10^{-32} cm^2 at a WIMP mass 50 GeV/c^2. The LZ experiment will observe an ER background, primarily from pp neutrinos, about 5 orders of magnitude lower than DAMA backgrounds, so LZ should achieve a limit, assuming background subtraction, of approximately 2×10^{38} cm^2. This sensitivity is comparable to the indirect astrophysical limits on the SD WIMP-electron scattering cross sections deduced from Super-Kamiokande data [22].

4.2.2 Axions and Axion-like Particles

The axion was introduced to describe the absence of CP-violation in the strong interaction. These particles, known as QCD axions, have a specific relationship between their mass and their coupling to fermions [28-30]. A particle with properties similar to the axion, but without the relationship between mass and fermion coupling, is known as an axion-like particle (ALP) [31].

The LZ experiment will be sensitive to axions and ALPs via the axioelectric effect, where an axion is absorbed and an atomic electron is ejected [32]. In contrast to the photoelectric effect, the mass of the axion or ALP is available for transfer to the atomic electron.

Two sources of axions or ALPs contribute to a possible signal in LZ [33]:

1. Nonrelativistic ALPs that might constitute the dark matter of our galaxy could cause signals in LZ, if their masses are sufficient to provide enough energy to ionize a Xe atom.
2. Axions or ALPs with a mass less than about 15 keV emitted by bremsstrahlung, Compton scattering, or other atomic processes in the sun also can ionize the Xe atoms in LZ [34].

Events caused by axions or ALPs in LZ would be ERs with energy up to a few tens of keV_{ee}. The neutrinos emitted by pp fusion in the sun will be the dominant background. The signal identification relies on the distinct shape of the energy spectrum of the axion or ALP signal.

The signal for a galactic dark-matter ALP would be a peak in ERs with energy at the mass of the particle. Our studies indicate that the LZ sensitivity to the coupling between electrons and galactic dark-matter ALPs ranges from a coupling constant g_{Ae} of 10^{-14} to one of 10^{-13}, for masses between 1 keV/c^2 and 20 keV/c^2, as shown in Figure 4.2.2.1.

The signal for solar ALPs is a broad thermal spectrum caused principally by bremsstrahlung and the Compton effect in the sun convolved with the axioelectric cross section. Our studies indicate that LZ is sensitive to a coupling constant g_{Ae} between solar ALPs and the electron of about 1.3×10^{-12} for masses between 0 keV/c^2 and approximately 1 keV/c^2, as shown in Figure 4.2.2.2.

4.2.3 Neutrino Physics

The LZ detector is sufficiently large and sensitive that neutrinos cause interesting signals that are uniform throughout the LXe volume, and which cannot be shielded. We have studied possible LZ observations of astrophysical, reactor, and geophysical neutrinos. Solar and atmospheric neutrinos have been studied as both signal and background to a WIMP search, and the prospective neutrino signal from a nearby supernova has been evaluated. LZ can make the first real-time observations of the neutrinos from pp fusion via elastic νe→νe scattering, and would be sensitive to the neutrino burst from a nearby supernova via the as-yet-unobserved

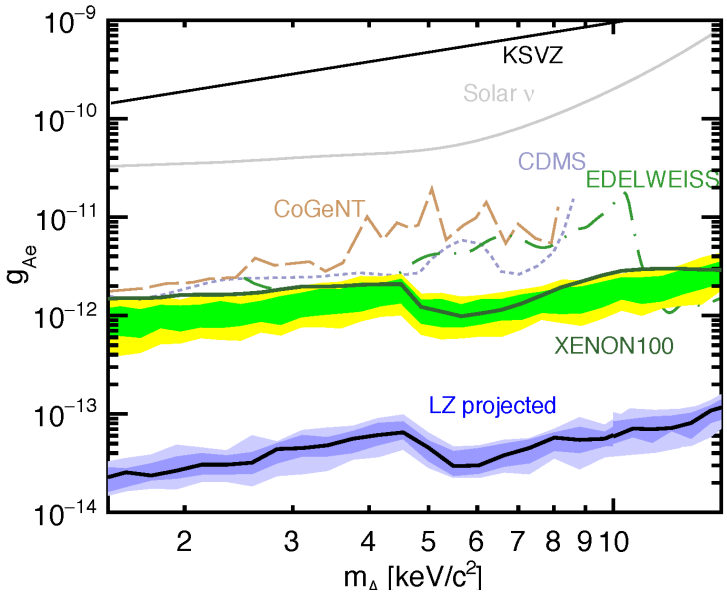

Figure 4.2.2.1. Dark-matter axion-like particle sensitivity. The LZ projected sensitivity for ALPs at 90% CL is shown by the dark/light blue bands, which show the 68%(1σ) and 95%(2σ) bands for that sensitivity. The line that defines KSVZ axions [35,36], an astrophysical upper limit from solar neutrinos [37], is shown. Upper limits by the experiments CDMS [38], EDELWEISS [39], CoGeNT [40], and XENON100 [41] are also shown.

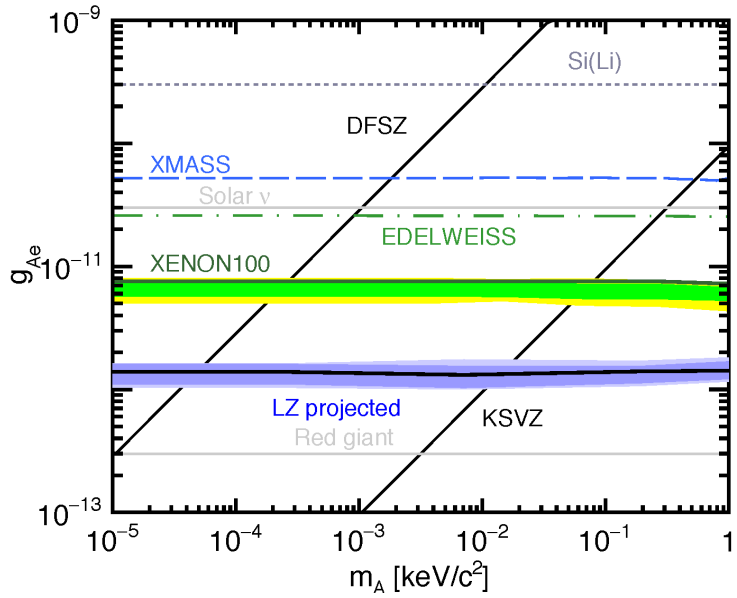

Figure 4.2.2.2. Solar axion-like particle sensitivity. Horizontal lines all extend down to m_A=0. The LZ projected sensitivity for ALPs at 90% CL is shown by the dark/light blue bands, which show the 68%(1σ) and 95%(2σ) bands for that sensitivity. The lines that define DFSZ axions [43,44] and KSVZ axions [35,36], astrophysical upper limits from solar neutrinos [37], and from red giants [45], are shown. Upper limits by the experiments XMASS [46], EDELWEISS [39], and XENON100 [41] are also shown.

process of coherent nuclear scattering. We have also estimated the potential of LZ to observe neutrinoless double-beta decay ($0\nu\beta\beta$) from ^{136}Xe, and considered the impact on the reactor/source neutrino anomaly and on searches for a neutrino magnetic moment of a prolonged exposure of LZ to a nearby ^{51}Cr neutrino source.

Most events in LZ from neutrino-related processes are ERs from solar neutrinos originating from the pp burning reaction in the sun [47,48], and also from the decay electrons from two-neutrino double-beta decay ($2\nu\beta\beta$) of ^{136}Xe [49]. For ER energies between 1.5 and roughly 20 keV$_{ee}$, ERs from pp solar neutrinos dominate [50], and contribute 850 observable events through $\nu e \rightarrow \nu e$ scattering in the LZ fiducial mass of 5.6 tonnes and a run of 1,000 days. We have neglected atomic effects that suppress the rate by of order 10% [51]. For ER energies above 20 keV$_{ee}$, ($2\nu\beta\beta$) events from ^{136}Xe dominate.

The LZ experiment alone compares very favorably with the existing world experimental data on pp solar neutrinos. The SAGE experiment, consisting of approximately 50 tonnes of gallium, observed 854 events attributed to pp solar neutrinos in 18 years of operations [52]. The SAGE experiment detected solar neutrinos via inverse beta decay, while LZ will detect solar neutrinos via $\nu e \rightarrow \nu e$ scattering. The threshold neutrino energy for LZ is 20 keV, while that of a gallium experiment is 233 keV, giving LZ sensitivity to a different portion of the pp fusion neutrino spectrum than was measured with SAGE. The LZ experiment will identify the time of pp solar neutrino events to a few nanoseconds, in contrast to the multiday time delay of the radiochemical process in SAGE.

Although the LZ experiment will open up new experimental territory in the study of pp solar neutrinos, the current consensus in the solar neutrino community is that the accuracy of pp solar neutrino measurement must be better than 1% to improve understanding of solar neutrinos [48]. To achieve 1% accuracy, LZ would need to observe several tens of thousands of pp neutrino-induced ER events, and also control systematics at a sub-1% level. Elimination of the ^{136}Xe isotope and a live time of 2,000 to 4,000 days would allow the accuracy of an LZ measurement of pp solar neutrinos to approach 1%.

The ERs from solar pp neutrinos, after the rejection in the S1+S2 analysis, are the largest source of background in the NR search region of LZ. However, there are also NR backgrounds originating from the as-yet-unobserved process of neutrino scattering that is coherent across nucleons in the nucleus [53,54]. For a given energy of the incident neutrino, the energy of the NR from coherent neutrino is typically suppressed by $\approx m_e/m_N$ relative to the energy of the analogous ER. Nuclei that recoil from solar pp neutrinos, and indeed from the entire spectrum of solar neutrinos, fall below the LZ S1+S2 analysis threshold of 6 keV$_{nr}$ [55,56]. The S2-only analysis should be sensitive to solar neutrinos from ^{8}B.

There are other sources of neutrinos (from the diffuse supernova neutrino background (DSNB) and from atmospheric neutrinos) with energies above the 19 MeV necessary to cause a Xe recoil above the LZ threshold, and below 50 MeV where scattering off of nucleons in the nucleus becomes incoherent. We estimate an irreducible background in the NR search region of 0.05 (DSNB) and 0.25 (atmospheric neutrinos) for an LZ fiducial mass of 5.6 tonnes and a run duration of 1,000 days.

The nearest power reactors are about 800 km away, in Fort Calhoun, NE (0.5 GWe), and Cooper, NE (0.8 GWe). The power/distance^2 distribution shows a broad peak for reactors in Illinois and Wisconsin. The net flux is small enough, however, that we expect negligible detected events from power-reactor neutrinos in LZ.

Geophysical neutrinos from ^{238}U and ^{232}Th decays have been seen by the KamLAND [57-59] and Borexino [60] detectors. Those detectors have an energy threshold for neutrinos of about 1.8 MeV. They are unable to detect neutrinos from the decay of ^{40}K, which have an energy just below 1.5 MeV. Using the Reference Earth Model and neutrino flux calculations from the KamLAND work, we estimate 1.5 ER events/year from ^{40}K decay, 0.3 ER events/year from ^{238}U decay, and 0.2 ER events/year from ^{232}Th decay. With LZ's ER/NR rejection ratio, these provide negligible backgrounds for the dark-matter search.

Should a supernova occur in our galaxy during LZ operation, neutrinos emitted from the supernova would be detected via coherent neutrino-nucleus scattering, which is blind with respect to neutrino flavor. The energy spectrum of neutrinos emitted from a typical supernova peaks near 10 MeV, and has a tail that extends above 50 MeV, which causes NRs above the LZ threshold [61]. Coherent neutrino-nucleus scattering is mediated by the weak neutral current, and thus provides important information on the flux and spectrum of muon and tau neutrinos from supernovae, complementary to the signals that would be seen in other detectors. From a supernova in our own galaxy at 10 kpc, LZ would see ~50 NR events of energy greater than 6 keV_{nr} in a rapid 10-sec burst [62,63]. The NR recoil spectrum increases as the recoil energy decreases; a threshold of 3 keV_{nr} would allow detection of ~100 supernova neutrino-induced NR events. The current world sample of 19 supernova neutrino-induced events were detected from supernova 1987a, 50 kpc from Earth, by detectors with total mass 1,200 times greater than LZ. A supernova 10 kpc from Earth would cause about 7,000 neutrino-induced events in the 32,000 tonnes of water in the Super-Kamiokande detector [61].

The sensitivity of LZ to neutrinoless double-beta decay of ^{136}Xe (Q-value 2,458 keV) depends strongly on the radioactivity levels achieved in detector materials and on the energy resolution of the combined S1+S2 signal (we note that LZ is not optimized for such large dynamic range). We have performed Monte Carlo simulations of various backgrounds for neutrinoless double-beta decay, and find that the most significant contributions are the 2,448-keV gamma line and the 2,614-keV gamma line, from ^{214}Bi and ^{208}Tl decay, respectively, which can penetrate deeply into the active region. The ^{60}Co sum peak (1,173 keV + 1,333 keV =2,506 keV) is also an important background, arising especially in stainless steel components. These gamma-ray backgrounds can be accurately measured using the full detector active mass, and can be substantially reduced through self-shielding and multiple scattering cuts. Solar neutrino and 2-neutrino double-beta decay backgrounds are found to be small in comparison. Energies are determined through an optimal linear combination of S1 and S2 signals, with a predicted 1-sigma energy resolution of 0.8% at the 2,458-keV Q-value. With a natural Xe target and 1,000 live days, LZ should be sensitive to ^{136}Xe half-lives from 2×10^{25} years to 2×10^{26} years, depending on achieved background, spatial, and energy resolution. The shorter value corresponds to an increase of 10 times over baseline radiopurity, an energy resolution of 2%, and a spatial resolution of 6 mm. Improvements in spatial and energy resolution, background reductions, and enriching the Xe target would improve these limits to perhaps 2×10^{27} years. For

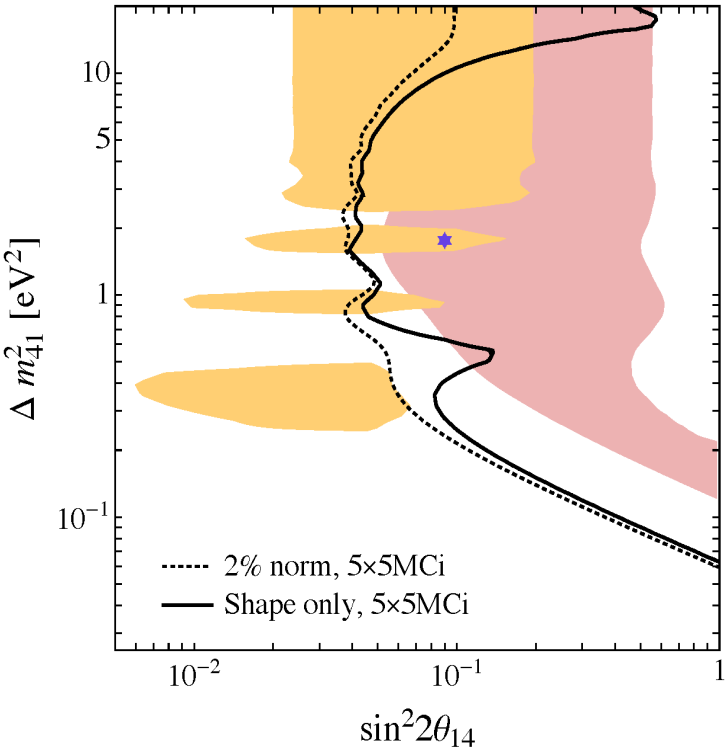

Figure 4.2.3.1. Sensitivity to sterile neutrino oscillations as a function of mass-difference and mixing angle. The parameter space to the right of each line would be excluded at 95% CL. The shaded areas show the 95% CL allowed regions for source (pink) and reactor (yellow) anomalies. The blue star is the joint best fit. The black solid line shows the expected contours for five 100-day deployments of a 5 MCi ^{51}Cr source next to LZ, without use of the source normalization. The dotted line shows the contour if a 2% normalization of the source is available. From Ref. [64].

comparison, the July 2012 half-life limit from EXO-200 [65] was 1.6×10^{25} years at 90% confidence limit, and KamLAND-Zen has placed a limit of 1.9×10^{25} years [66].

There are long-standing anomalies arising from the detailed study of antineutrinos from reactors, and from source-calibration of solar neutrino experiments [67]. A recent study has evaluated the capabilities of deployment of a 5 MCi ^{51}Cr electron neutrino source near to the LZ detector [64]. The excellent spatial resolution of the LXe TPC allows the spatial pattern of electron neutrino oscillation into a sterile neutrino to be detected. A neutrino source experiment with LZ would not be part of the principal LZ science goal, which is the WIMP search, and would constitute a distinct follow-on experiment after the WIMP search had achieved significant results.

The sensitivity achievable by five source deployments of a 5 MCi ^{51}Cr source near LZ is shown in Figure 4.2.3.1. Numerous proposals are under way to probe the origin of the reactor/source anomalies [68], but the potential LZ advantage is a diminished need to control the source normalization due to LZ's excellent spatial resolution. In addition, a source deployment near LZ will bring sensitivity to an electron neutrino magnetic moment that is close to the limits deduced from astrophysical considerations [64].

4.3 Key Requirements

In this section, we summarize the key high-level requirements and their dependence on some of the critical detector performance assumptions. The LZ collaboration has established a small number of such requirements to guide and evaluate the design and later fabrication of the detector systems. The top-level scientific requirement is the sensitivity to WIMPs. Subsidiary high-level science requirements and the flow-down from the overall sensitivity are shown in Figure 4.3.1. The high-level requirements, including the key infrastructure requirements, are summarized in Table 4.3.1. These requirements flow down to the detector subsystems and are captured in a concise form available to the collaboration. There are two practical high-level requirements. First, all equipment and subassemblies must be transported via the Yates shaft (see Chapter 13), which imposes dimensional and weight limits. Second, the existing water tank now housing the LUX detector must be reused (rather than be made anew).

The collaboration has also captured the requirements for detector subsystems at WBS level 2. There is a well-identified process for requirements flow-down and verification that will be used first in the design phase and then in the fabrication (or installation) phase.

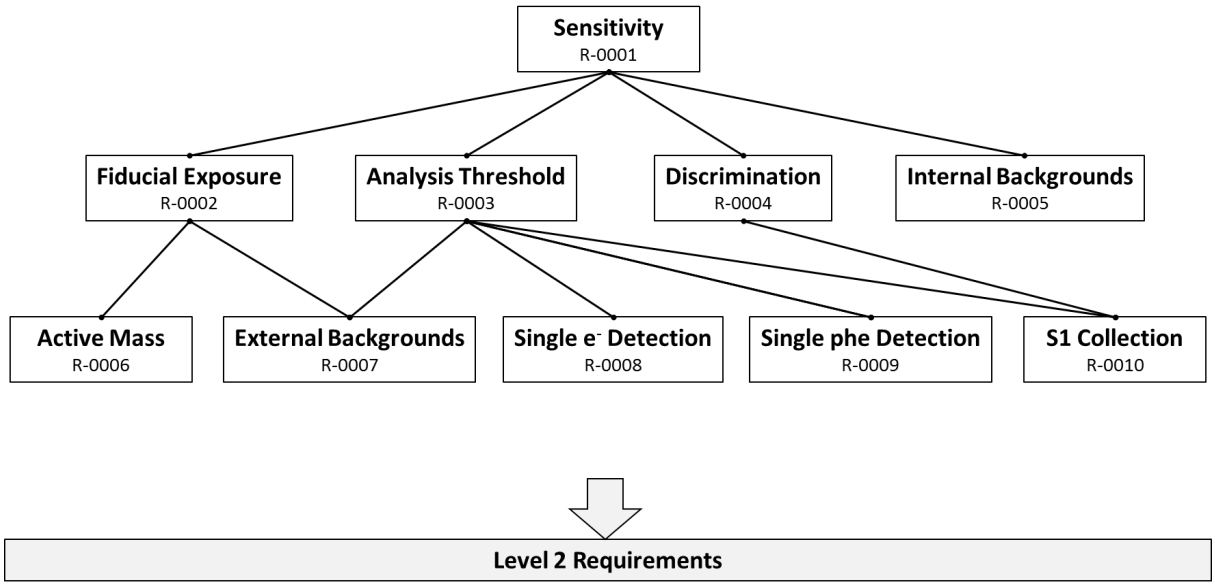

Figure 4.3.1. High-level science requirements, leading to the overall sensitivity to WIMPs.

Table 4.3.1. Summary of high-level requirements established by LZ to guide the design and fabrication of the experiment.

Requirement Number	Type	Name	Value	Description
Primary				
R-0001	Science	WIMP Sensitivity	Sensitivity to 50 GeV/c^2 WIMPs is 2 x 10^{-48} cm^2 or better.	Probe limit of LXe technology set by solar neutrino background. Approach sensitivity to atmospheric neutrinos. Test prominent supersymmetric and extra-dimension models of dark matter.
Secondary				
R-0002	Science	Fiducial Exposure	5,600 tonne-days	Minimum fiducial mass of 5.6 tonnes and assumed running period of 1,000 live days.
R-0003	Science	Analysis Threshold	50% efficiency at 6 keVnr	Probe WIMP mass range down to 5 GeV with non-negligible sensitivity.
R-0004	Science	ER Discrimination	99.5%	Limit background from ERs so as to reach WIMP sensitivity requirement. NR acceptance 50%.
R-0005	Science	Internal Backgrounds	ER events from Kr+Rn <20% of pp solar neutrino ER rate	Limit ERs from internal backgrounds to be significantly less than ERs from solar neutrinos.
Tertiary				
R-0006	Science	Active Mass	7.0 tonnes	Required to reach fiducial exposure
R-0007	Science	External Backgrounds	Backgrounds from radioactivity of the detector components (not including internal backgrounds, R-0005). ER counts before discrimination <21. NR counts ≤0.1	ER counts constrained to be <10% of ERs from solar neutrinos, including uncertainty in this rate. NR events constrained to be small in comparison to total background. We rely on veto efficiency to reduce the NR rate contribution. This rate, and to a lesser extent external ER contributions, define the fiducial mass. Analysis threshold also depends on size of these backgrounds.
R-0008	Science	Single Electron Detection	50 photoelectrons detected per emitted electron	Sufficiently large S2 signal for accurate reconstruction of peripheral interactions, such as those arising from contamination on the TPC walls.
R-0009	Science	Single Photoelectron Detection	Single S1 photoelectron detection with >90% efficiency, so as to reach >70% efficiency for 3 phe	Main determinant of analysis threshold
R-0010	Science	S1 Light Collection	Volume-averaged S1 photon-detection efficiency (geometric light-collection times effective PMT quantum efficiency) of ≥7.5%	Good discrimination and low-energy threshold, equal to or better than past Xe experiments. Exponentially falling (in recoil energy) WIMP spectrum means more recoils at lower energies, and low-energy recoils produce less S1 (both total and per-unit-energy) driving the S1 light collection efficiency requirement.

Requirement Number	Type	Name	Value	Description
Infrastructure				
R-0100	General	All parts fit down Yates shaft	All detector elements must be sized so that they can be lowered via the Yates shaft.	Yates shaft is primary access to the Davis Campus.
R-0110	General	Reuse Davis water tank	Existing Davis water tank is reused. Include minor modifications and refurbishment.	Not practical or cost-effective to replace water tank. Insufficient underground space to make larger tank.

Requirements validation is a key element of internal reviews of LZ detector systems and will be an important aspect of configuration control.

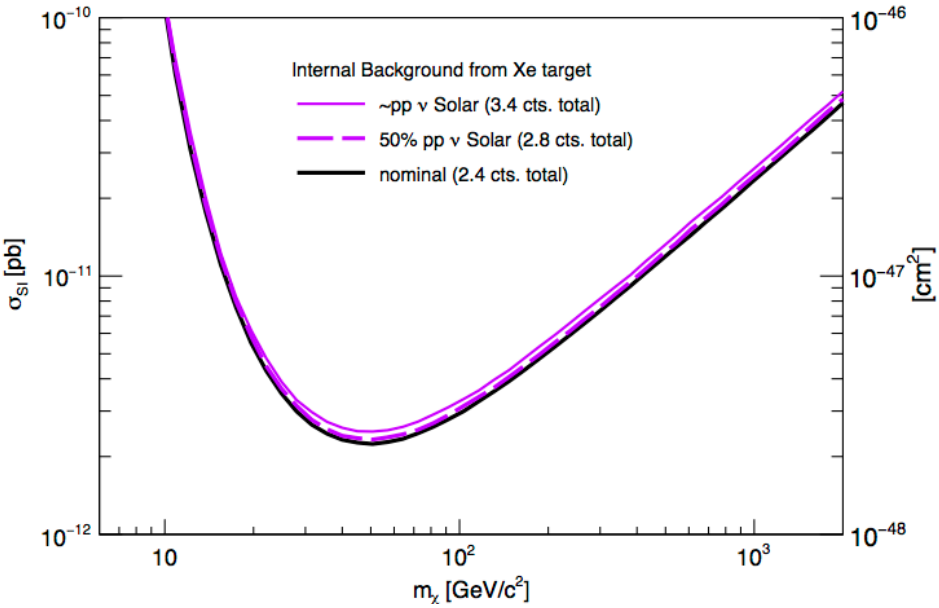

Figure 4.3.2. Sensitivity if internal backgrounds (Kr and Rn) increase beyond baseline assumptions.

We have examined the dependency of the LZ sensitivity on some critical performance assumptions and present key parts of these studies of below. The projected sensitivity for the baseline fiducial exposure of 5,600 tonne-days was shown in Figure 4.1.1.2, and the dependence of the sensitivity on less and more fiducial exposure is given in Figure 4.1.1.4. Even if the ER discrimination is poorer than the baseline assumption (99.5%), we can likely achieve the sensitivity requirement by additional running time.

The dependence of the background (with baseline background assumptions) in case the ER discrimination is better than 99.5% or lower at 99.1% is given in Table 4.1.1.2. Our assumption of 99.5% ER discrimination is conservative, and better discrimination would somewhat reduce the overall background levels. Conversely, ER discrimination somewhat poorer than the baseline would have a modest degrading effect and require more running time, as noted above.

Our baseline assumptions of internal Kr and Rn backgrounds are shown in Table 3.8.1.1. The dependence of the sensitivity in case these internal backgrounds increase is shown in Figure 4.3.2. These backgrounds, particularly Rn, are among the most difficult to control but we are not near a critical point with our baseline assumption, which is 10% of the pp solar neutrino rate.

Our baseline assumptions for key external backgrounds are also given in Table 3.8.1.1. The dependence of the sensitivity in case the external backgrounds increase is given in Figure 4.3.3. Note that the baseline backgrounds correspond to about 10% of the pp neutrino solar background. We have prudent headroom in case the external backgrounds are larger than our baseline assumptions.

The approximate dependence of the sensitivity on active mass is given in Figure 4.3.4. This is calculated from a simple right-cylinder model of obtaining the fiducial volume from the baseline 7-tonne active volume, and then simple scaling for smaller volumes. We note that at least the full 7-tonne active volume and three years of operation are required to start to be sensitive to the neutrino background at larger WIMP masses.

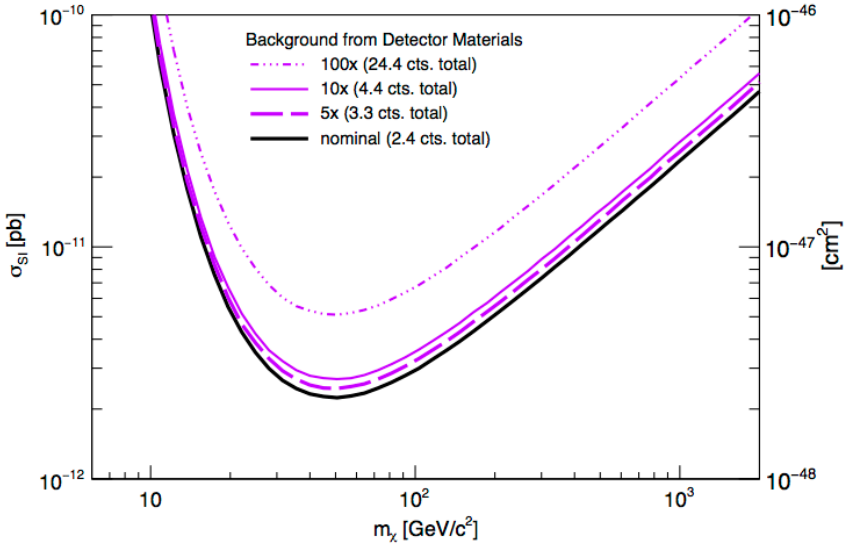

Figure 4.3.3. Sensitivity if external backgrounds increase beyond baseline assumptions.

Our baseline assumption for the average S1 light collection is 7.5%. The light-collection efficiency affects the ER discrimination, which is discussed in more detail in Chapter 6. The dependence of the sensitivity on average light collection is shown in Figure 4.3.5. For example, a reduction in light-collection efficiency to 4% would yield an ER discrimination of 99.1%, and the effect of this has been described previously. The effects of changes to the single-electron and single-photoelectron detection efficiency are also discussed in more detail in Chapter 6. The dependence of the sensitivity on the single-photoelectron detection efficiency is shown in Figure 4.3.6.

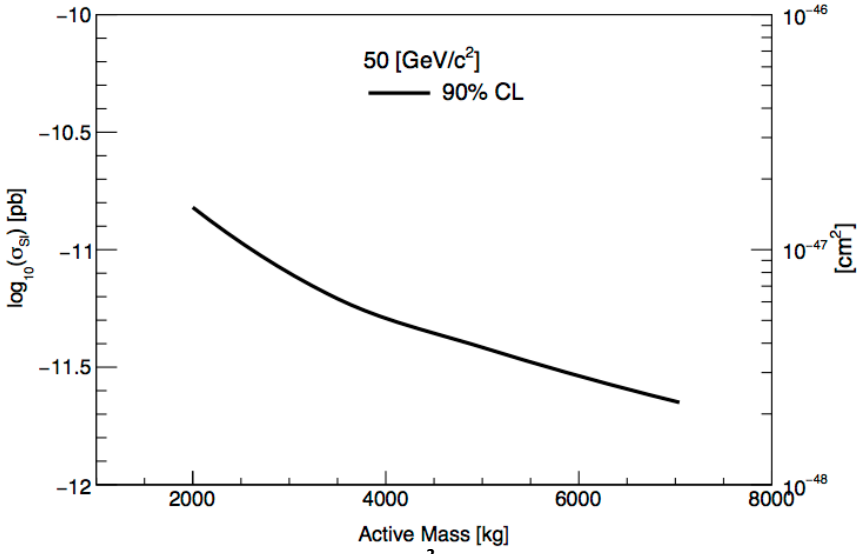

Figure 4.3.4. Sensitivity at 50 GeV/c^2 as a function of the total active Xe mass.

The sensitivity also could be affected by the purity of the xenon. The dependence of the sensitivity on the characteristic drift times is shown in Figure 4.3.7. There is significant margin, unless the drift time becomes less than one-half the nominal value. We note that drift times in excess of 500 microseconds have routinely been obtained in LUX.

Finally, we show in Figure 4.3.8 both the nominal sensitivity and a curve representing a 3σ discovery.

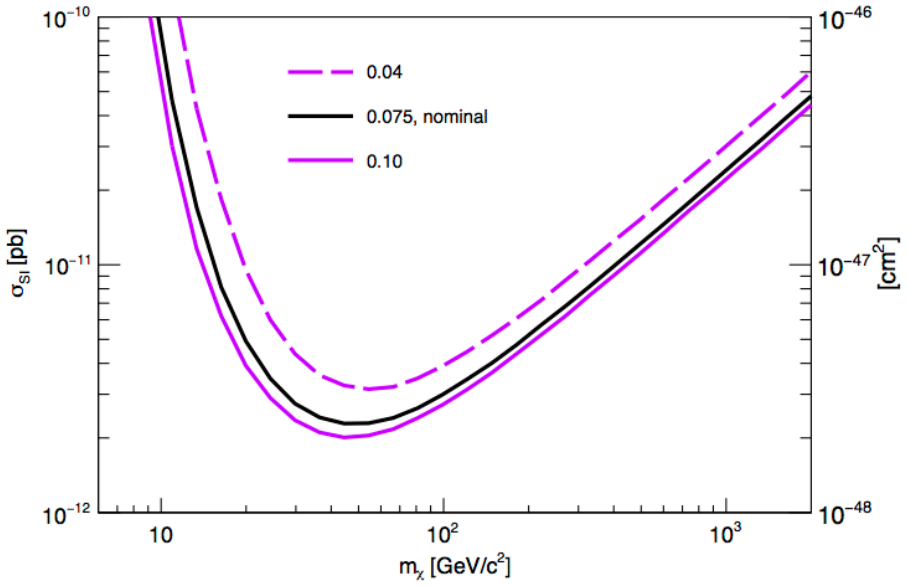

Figure 4.3.5. Dependence of the sensitivity on the average light collection as it varies from 4% to 10%. The baseline value is 7.5%.

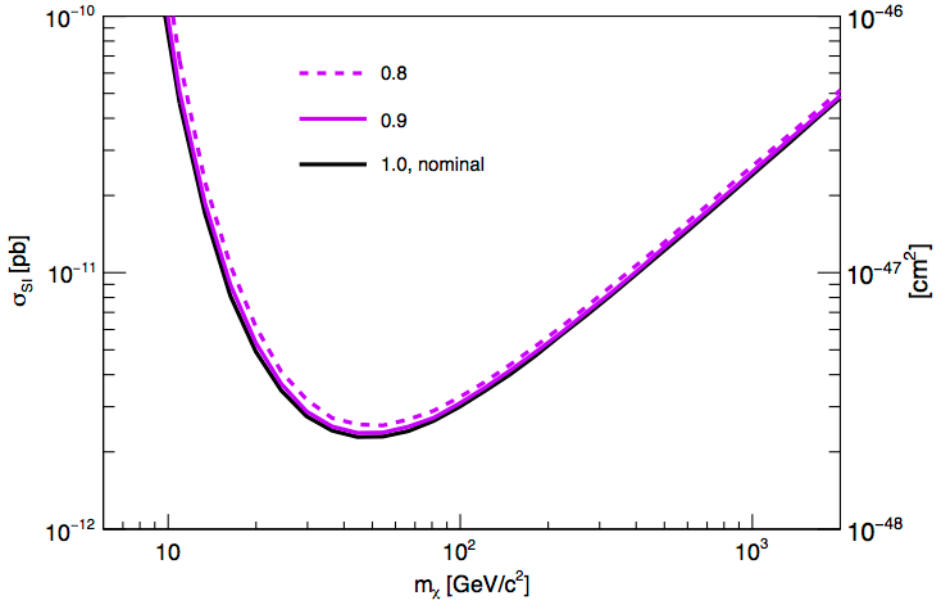

Figure 4.3.6. Dependence of the sensitivity on the single photoelectron detection efficiency.

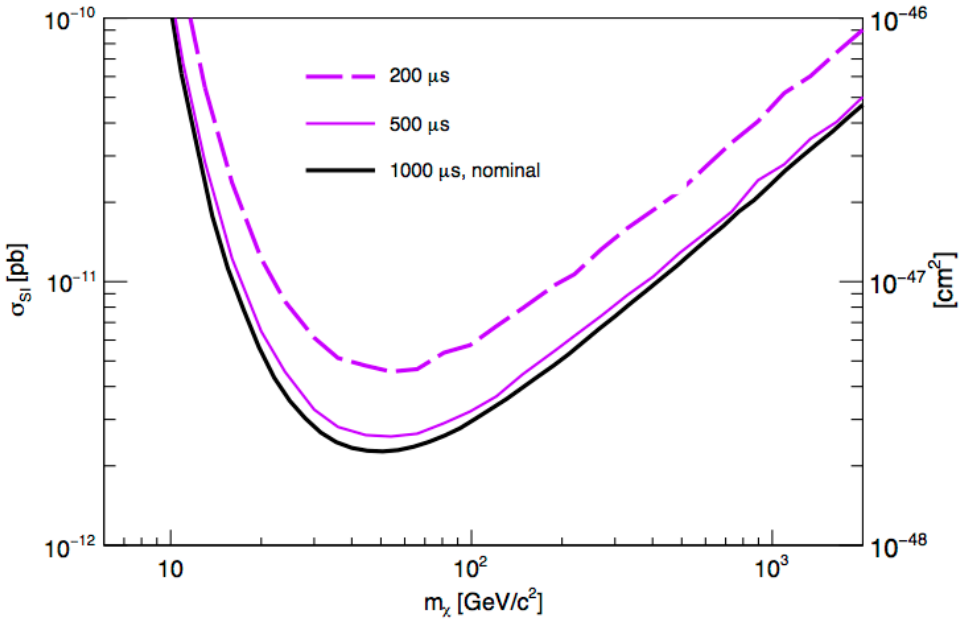

Figure 4.3.7. Dependence of the sensitivity on the characteristic drift time.

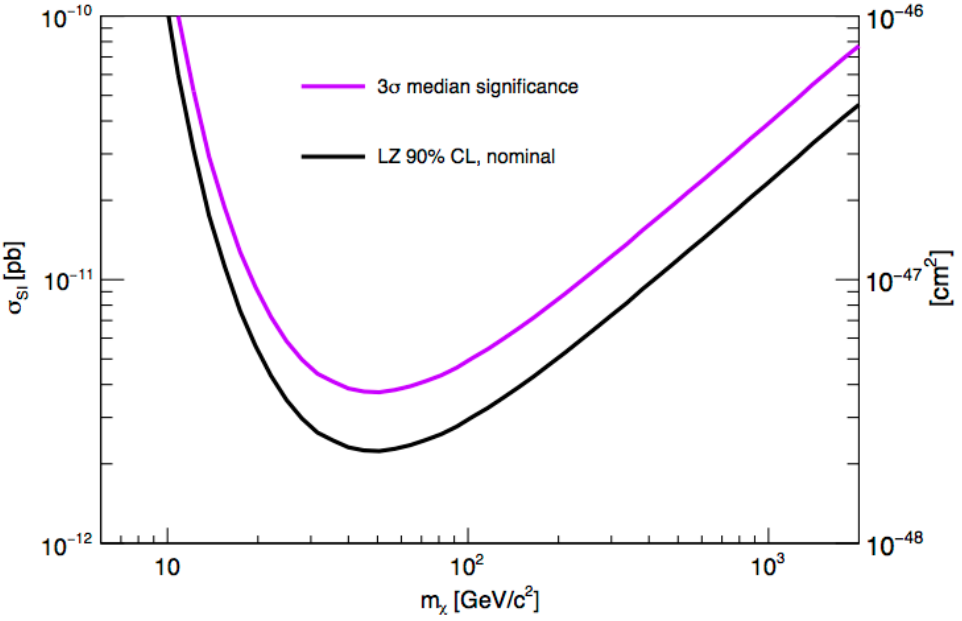

Figure 4.3.8. The nominal sensitivity 90% confidence level limit and a 3σ significance discovery potential.

Chapter 4 References

[1] M. Pato, L. E. Strigari, R. Trotta, and G. Bertone, J. Cosmol. Astropart. Phys. **2013**, 041 (2013), arXiv:1211.7063 [astro-ph].

[2] D. S. Akerib *et al.* (LUX), Phys. Rev. Lett. **112**, 091303 (2014), arXiv:1310.8214 [astro-ph].

[3] R. Barbieri, M. Frigeni, and G. F. Giudice, Nucl. Phys. **B313**, 725 (1989).

[4] M. A. Shifman, A. I. Vainshtein, and V. I. Zakharov, Phys. Lett. **B78**, 443 (1978).

[5] J. Billard, L. Strigari, and E. Figueroa-Feliciano, Phys. Rev. **D89**, 023524 (2014), arXiv:1307.5458 [hep-ph]; F. Ruppin, J. Billard, E. Figueroa-Feliciano, and L. Strigari, Phys. Rev. **D90**, 083510 (2014), arXiv:1408.3581 [hep-ph].

[6] J. D. Lewin and P. F. Smith, Astropart. Phys. **6**, 87 (1996).

[7] C. McCabe, Phys. Rev. **D82**, 023530 (2010), arXiv:1005.0579 [hep-ph].

[8] L. Roszkowski, E. M. Sessolo, and A. J. Williams, J. High Energy Phys. **2014**, 067 (2014), arXiv:1405.4289 [hep-ph].

[9] C. Strege, G. Bertone, G. J. Besjes, S. Caron, R. Ruiz de Austri, A. Strubig, and R. Trotta, J. High Energy Phys. **2014**, 081 (2014), arXiv:1405.0622 [hep-ph].

[10] E. Santos *et al.* (ZEPLIN-III), J. High Energy Phys. **2011**, 115 (2011), arXiv:1110.3056 [physics.ins-det].

[11] G. Jungman, M. Kamionkowski, and K. Griest, Phys. Rept. **267**, 195 (1996), arXiv:hep-ph/9506380 [hep-ph].

[12] A. L. Fitzpatrick, W. Haxton, E. Katz, N. Lubbers, and Y. Xu, J. Cosmol. Astropart. Phys. **2013**, 004 (2013), arXiv:1203.3542 [hep-ph].

[13] M. W. Goodman and E. Witten, Phys. Rev. **D31**, 3059 (1985).

[14] A. Kurylov and M. Kamionkowski, Phys. Rev. **D69**, 063503 (2004), arXiv:hep-ph/0307185 [hep-ph].

[15] G. Bélanger, E. Nezri, and A. Pukhov, Phys. Rev. **D79**, 015008 (2009), arXiv:0810.1362 [hep-ph].

[16] J. L. Feng, J. Kumar, D. Marfatia, and D. Sanford, Phys. Lett. **B703**, 124 (2011), arXiv:1102.4331 [hep-ph].

[17] P. Cushman *et al.*, in *Planning the Future of U.S. Particle Physics, The Snowmass 2013 Proceedings*, edited by N. A. Graf, M. E. Peskin, and J. L. Rosner (2013); Working Group Report:*WIMP Dark Matter Direct Detection*, arXiv:1310.8327 [hep-ex].

[18] D. R. Tovey, R. J. Gaitskell, P. Gondolo, Y. A. Ramachers, and L. Roszkowski, Phys. Lett. **B488**, 17 (2000), arXiv:hep-ph/0005041 [hep-ph].

[19] P. Klos, J. Menéndez, D. Gazit, and A. Schwenk, Phys. Rev. **D88**, 083516 (2013), [Erratum: Phys. Rev. **D89**, 029901 (2014)], arXiv:1304.7684 [nucl-th].

[20] M. Garny, A. Ibarra, M. Pato, and S. Vogl, Phys. Rev. **D87**, 056002 (2013), arXiv:1211.4573 [hep-ph].

[21] L. Baudis, G. Kessler, P. Klos, R. F. Lang, J. Menéndez, S. Reichard, and A. Schwenk, Phys. Rev. **D88**, 115014 (2013), arXiv:1309.0825 [astro-ph].

[22] T. Tanaka *et al.* (Super-Kamiokande), Astrophys. J. **742**, 78 (2011), arXiv:1108.3384 [astro-ph].

[23] M. G. Aartsen *et al.* (IceCube), Phys. Rev. Lett. **110**, 131302 (2013), arXiv:1212.4097 [astro-ph].

[24] M. I. Gresham and K. M. Zurek, Phys. Rev. **D89**, 123521 (2014), arXiv:1401.3739 [hep-ph].

[25] R. Catena and P. Gondolo, J. Cosmol. Astropart. Phys. **2014**, 045 (2014), arXiv:1405.2637 [hep-ph].

[26] J. Kopp, V. Niro, T. Schwetz, and J. Zupan, Phys. Rev. **D80**, 083502 (2009), arXiv:0907.3159 [hep-ph].

[27] R. Bernabei *et al.* (DAMA), *Nuclear Physics in Astrophysics. Proceedings, 17th International Conference, NPDC 17, Debrecen, Hungary, September 30 to October 4, 2002*, Nucl. Phys. **A719**, 257 (2003), *Searching for the dark universe by the DAMA experiment*.

[28] R. D. Peccei and H. R. Quinn, Phys. Rev. Lett. **38**, 1440 (1977).

[29] S. Weinberg, Phys. Rev. Lett. **40**, 223 (1978).

[30] F. Wilczek, Phys. Rev. Lett. **40**, 279 (1978).

[31] K. A. Olive *et al.* (Particle Data Group), Chin. Phys. **C38**, 090001 (2014), Review of Particle Physics: *Gauge and Higgs Bosons,* A. Ringwald, L.J Rosenberg, and G. Rybka, *Axions and Other Similar Particles,* pp. 626-635.

[32] S. Dimopoulos, G. D. Starkman, and B. W. Lynn, Phys. Lett. **B168**, 145 (1986).

[33] K. Arisaka, P. Beltrame, C. Ghag, J. Kaidi, K. Lung, A. Lyashenko, R. D. Peccei, P. Smith, and K. Ye, Astropart. Phys. **44**, 59 (2013), arXiv:1209.3810 [astro-ph].

[34] J. Redondo, J. Cosmol. Astropart. Phys. **2013**, 008 (2013), arXiv:1310.0823 [hep-ph].

[35] J. E. Kim, Phys. Rev. Lett. **43**, 103 (1979).

[36] M. A. Shifman, A. I. Vainshtein, and V. I. Zakharov, Nucl. Phys. **B166**, 493 (1980).

[37] P. Gondolo and G. Raffelt, Phys. Rev. **D79**, 107301 (2009), arXiv:0807.2926 [astro-ph].

[38] Z. Ahmed *et al.* (CDMS), Phys. Rev. Lett. **103**, 141802 (2009), arXiv:0902.4693 [hep-ex].

[39] E. Armengaud *et al.* (EDELWEISS-II), J. Cosmol. Astropart. Phys. **2013**, 067 (2013), arXiv:1307.1488 [astro-ph].

[40] C. E. Aalseth *et al.* (CoGeNT), Phys. Rev. Lett. **101**, 251301 (2008), [Erratum: Phys. Rev. Lett. 102,109903(2009)], arXiv:0807.0879 [astro-ph].

[41] E. Aprile *et al.* (XENON100), Phys. Rev. **D90**, 062009 (2014), arXiv:1404.1455 [astro-ph].

[42] M. Pospelov, A. Ritz, and M. B. Voloshin, Phys. Rev. **D78**, 115012 (2008), arXiv:0807.3279 [hep-ph].

[43] A. R. Zhitnitsky, Sov. J. Nucl. Phys. **31**, 260 (1980), [Yad. Fiz. 31, 497 (1980)].

[44] M. Dine, W. Fischler, and M. Srednicki, Phys. Lett. **B104**, 199 (1981).

[45] G. G. Raffelt, in *Axions: Theory, Cosmology, and Experimental Searches, Proceedings, 1st Joint ILIAS-CERN-CAST Axion Training, Geneva, Switzerland, November 30-December 2, 2005*, Lect. Notes Phys., Vol. **741** (2008) pp. 51–71, *Astrophysical Axion Bounds*, arXiv:hep-ph/0611350 [hep-ph].

[46] K. Abe *et al.* (XMASS-I), Phys. Lett. **B724**, 46 (2013), arXiv:1212.6153 [astro-ph].

[47] J. N. Bahcall and C. Peña-Garay, New J. Phys. **6**, 63 (2004), arXiv:hep-ph/0404061 [hep-ph].

[48] W. C. Haxton, R. G. Hamish Robertson, and A. M. Serenelli, Ann. Rev. Astron. Astrophys. **51**, 21 (2013), arXiv:1208.5723 [astro-ph].

[49] J. B. Albert *et al.* (EXO-200), Phys. Rev. **C89**, 015502 (2014), arXiv:1306.6106 [nucl-ex].

[50] L. Baudis, A. Ferella, A. Kish, A. Manalaysay, T. Marrodan Undagoitia, and M. Schumann, J. Cosmol. Astropart. Phys. **2014**, 044 (2014), arXiv:1309.7024 [physics.ins-det].

[51] G. J. Gounaris, E. A. Paschos, and P. I. Porfyriadis, Phys. Rev. **D70**, 113008 (2004), arXiv:hep-ph/0409053 [hep-ph].

[52] J. N. Abdurashitov *et al.* (SAGE), Phys. Rev. **C80**, 015807 (2009), arXiv:0901.2200 [nucl-ex].

[53] D. Z. Freedman, Phys. Rev. **D9**, 1389 (1974).

[54] B. Cabrera, L. M. Krauss, and F. Wilczek, Phys. Rev. Lett. **55**, 25 (1985).

[55] L. E. Strigari, New J. Phys. **11**, 105011 (2009), arXiv:0903.3630 [astro-ph].

[56] J. Billard, L. Strigari, and E. Figueroa-Feliciano, Phys. Rev. **D89**, 023524 (2014), arXiv:1307.5458 [hep-ph].

[57] E. Sanshiro, *Neutrino Geophysics and Observation of Geo-Neutrinos at KamLAND*, Ph.D. thesis, Tohoku University (2005).

[58] T. Araki *et al.*, Nature **436**, 499 (2005).

[59] S. Enomoto, E. Ohtani, K. Inoue, and A. Suzuki, Earth Planet. Sc. Lett. **258**, 147 (2007).

[60] G. Bellini *et al.* (Borexino), Phys. Lett. **B687**, 299 (2010), arXiv:1003.0284 [hep-ex].

[61] K. Scholberg, Ann. Rev. Nucl. Part. Sci. **62**, 81 (2012), arXiv:1205.6003 [astro-ph].

[62] C. J. Horowitz, K. J. Coakley, and D. N. McKinsey, Phys. Rev. **D68**, 023005 (2003), arXiv:astro-ph/0302071 [astro-ph].

[63] S. Chakraborty, P. Bhattacharjee, and K. Kar, Phys. Rev. **D89**, 013011 (2014), arXiv:1309.4492 [astro-ph].

[64] P. Coloma, P. Huber, and J. M. Link, J. High Energy Phys. **2014**, 042 (2014), arXiv:1406.4914 [hep-ph].

[65] M. Auger *et al.* (EXO), Phys. Rev. Lett. **109**, 032505 (2012), arXiv:1205.5608 [hep-ex].

[66] A. Gando *et al.* (KamLAND-Zen), Phys. Rev. Lett. **110**, 062502 (2013), arXiv:1211.3863 [hep-ex].

[67] K. N. Abazajian *et al.*, "Light Sterile Neutrinos: A White Paper," (2012), arXiv:1204.5379 [hep-ph].

[68] B. Caccianiga, in *XXVI INTERNATIONAL CONFERENCE ON NEUTRINO PHYSICS AND ASTROPHYSICS: Neutrino 2014*, AIP Conf. Proc., Vol. 1666 (2015) p. 180002, *Future short baseline neutrino searches with nuclear decays*; D. Lhuillier, in *XXVI INTERNATIONAL CONFERENCE ON NEUTRINO PHYSICS AND ASTROPHYSICS: Neutrino 2014*, Vol. 1666 (2015) p. 180003, *Future short-baseline sterile neutrino searches with reactors*.